Visualizations of 2D Temperature Distribution of Molten Metal in Arc Welding Process†

TANAKA Manabu*, WAKI Kenji, TASHIRO Shinichi***, NAKATA Kazuhiro****, YAMAMOTO Eri*****, YAMAZAI Kei***** and SUZUKI Keiichi*****

Abstract

In the present research, a general-purpose method for measurement and visualization of the temperature distribution of an object in arc welding, such as a tungsten electrode and a weld pool in GTA welding, and also a metal droplet and a weld pool in GMA welding, was conducted. Two-color pyrometry is utilized to obtain the temperature of the object. The object is photographed by high speed camera during arc welding. Two wave lengths (950 nm and 980 nm) in the infrared range are selected from the thermal radiation emitted from the object by using an imaging spectroscope, and the temperature is obtained from the intensity ratio of the two waves of radiation. Consequently, it was seen that in CO_2 arc welding, the 2D temperature distribution of the metal droplet is not uniform, namely, ranging from 2000 K to over 3000 K, while the 2D temperature distribution of the weld pool is more uniform, about 1800 K. It was found that there is a great difference between the temperature of the metal droplet and that of the weld pool in GMA welding process.

KEY WORDS: (Visualization), (Arc), (Temperature), (Measurement)

1. Introduction

Two-color pyrometry is utilized to obtain the temperature of an object from the radiation intensity ratio between two adjacent wavelengths assuming the same emissivity at each wavelength. The radiation intensity ratio is expressed referring to Planck's formula of radiation in the following equation.

$$\frac{I_1}{I_2} = \frac{\varepsilon_2}{\varepsilon_1}\left(\frac{\lambda_2}{\lambda_1}\right)^5 \frac{1-\exp\left(C_b/\lambda_2 T\right)}{1-\exp\left(C_b/\lambda_1 T\right)} \quad (1)$$

where, I: Intensity of radiation ($Wm^{-3}sr^{-1}$); ε : emissivity; λ : wavelength (nm); T: temperature (K); Cb: 0.014388 (mK) [1] .

Equation (2) shows that the temperature of the object can be determined by measuring the radiation intensity ratio assuming $\varepsilon_1 = \varepsilon_2$ in Equation (1).

$$\frac{I_1}{I_2} = \left(\frac{\lambda_2}{\lambda_1}\right)^5 \frac{\exp\left(C_b/\lambda_2 T\right)}{\exp\left(C_b/\lambda_1 T\right)} \quad (2)$$

Two-color pyrometry is well known as a non-contact type thermometry without requiring material emissivity. Especially in thermal spraying process, two-color pyrometry is conventionally employed and temperatures of flying particles[2-6] and particles split on the substrate surface[7] are measured with high accuracy. Furthermore, a special instrument （DPV-2000, Tecnar） enables the measurement of the particle diameter and velocity of the particle simultaneously in addition to the temperature[8].

In arc welding processes, targets of temperature measurement are the tungsten rod, the droplet at the tip of the welding wire and the weld pool of the base metal, those have function as an electrode in the arc discharge [9]. In the arc welding process, constriction of the thermal plasma generated by the arc discharge is required to melt the base metal and welding wire working as an electrode. In order to realize the constriction, a short electrode gap (2~5mm) is generally employed.

Two-color pyrometry is suitable for plasma spraying process, because the plasma radiation is relatively weak due to the long distance between torch nozzle and

† Received on December 18, 2009
* Professor
**KAWASAKI HEAVY INDUSTRIES, LTD.
***Assistant professor
****Professor
*****KOBE STEEL, LTD.

Transactions of JWRI is published by Joining and Welding Research Institute, Osaka University, Ibaraki, Osaka 567-0047, Japan

substrate. However, the electrodes to be the target are covered with high density thermal plasma in the arc welding process. It is difficult to apply two-color pyrometry to arc welding processes, since metal vapor evaporated from weld pool and the droplet at the tip of the wire drastically increases plasma radiation as shown in **Figure 1** [10, 11]. For this reason, conventionally, average temperature of the droplet was estimated from the heat quantity of the droplet [12] and a point of the weld pool temperature was measured by employing a thermocouple [13] in the arc welding process.

Applications of two-color pyrometry to arc welding process have been reported [14-16]. For example Haidar measured surface temperatures of tungsten electrodes in gas tungsten arc with high accuracy by employing a large spectroscope (focal length of 1m) and optical mirrors and lens for eliminating the plasma radiation and it's reflection on the electrode surface [14,15].

On the other hand, Hirata measured droplet temperatures in gas metal arc welding with two-color pyrometry. 2D images of the droplet at the wavelengths of 689nm and 590.2nm were simultaneously recorded by employing a pair of CCD cameras and interference filters just after the short circuiting transfer. 2D surface temperature distribution was calculated from the radiation intensity ratio. However, since plasma radiation is very strong in the visible ray range, the measurement can be conducted only at low arc current. Furthermore, only one temperature distribution can be obtained in each experiment due to the limitation of the CCD cameras.

Recently, it has become easy to apply two-color pyrometry to the arc welding process because of the remarkable improvement of personal computers, software and CCD cameras (frame rate, the number of pixels and dynamic range etc). In this paper, visualizations of 2D temperature distribution of molten metal in arc welding processes are introduced.

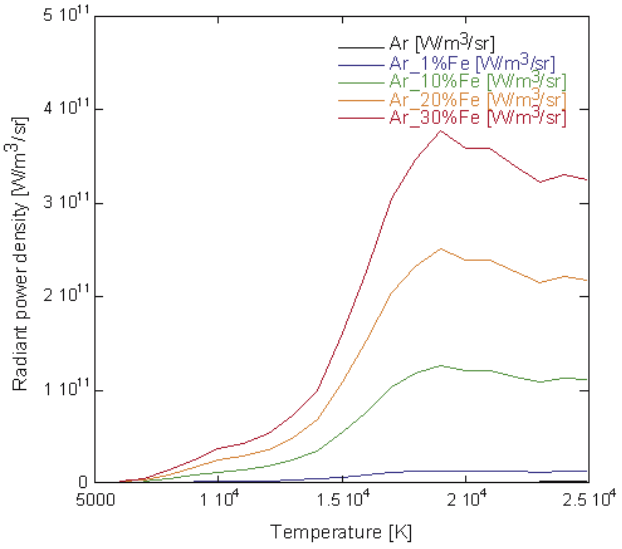

Fig. 1 Dependence of radiant power density of helium gas on temperature for each mixing ratio.

2. High-speed temperature measurement system by two-color pyrometry

A schematic illustration and a photograph of high-speed temperature measurement system using two-color pyrometry are shown in **Figure 2** and **Figure 3**, respectively. A virtual image formed in the optical system by the object lens is duplicated as two identical images with the branch mirror (Photron , Multi-Spectral-Imager). These images pass through the interference filters (950 nm, 980 nm) and are recorded with the sensor (Photron, FASTCAM-512PCI) as the images at wavelengths of 950nm and 980nm, respectively. In this study, the relationship between radiation intensity ratio and temperature was calibrated by employing a tungsten lamp calibrated by JCSS (Japan Calibration Service System) as a standard lamp. Temperature data was calculated from the radiation intensity ratio data for each pixel referring this calibration data. It is well known that the plasma radiation is mostly in the ultra-violet ray range (especially 200 nm~400 nm) and, conversely, it is very weak in the infrared ray range. Therefore, the wavelengths of 950nm and 980nm in the infrared ray range are selected to eliminate influence of the plasma radiation.

In order to evaluate the reliability of the high-speed temperature measurement system by two-color pyrometry, measurement of surface temperature of a tungsten electrode in the gas tungsten arc was conducted. The cathode image was recorded just after switching off the arc from a steady state (arc current of 200A) at a frame rate of 5000fps. The experimental result of cathode surface temperature distribution is shown in **Figure 4**. For comparison, the temperature during arc operation measured by Haidar was also plotted[15]. Experimental conditions such as shape of tungsten electrode, arc current, arc gap and composition of shielding gas are the same as those of Haidar. It was found that the temperature just after switching off the arc is nearly the same level as that during arc operation because the temperature measured in this experiment agrees with that of Haidar. Experimental error ($\Delta T/T$) of this system is estimated to be ±5% from the temperature difference of 100K at the tip of the electrode.

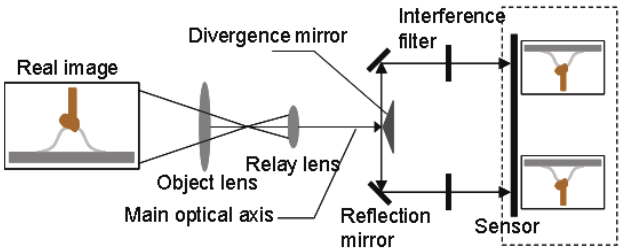

Fig. 2 Schematic illustration of high-speed temperature measurement system by two-color pyrometry.

Fig. 3 Photograph of high-speed temperature measurement system by two-color pyrometry.

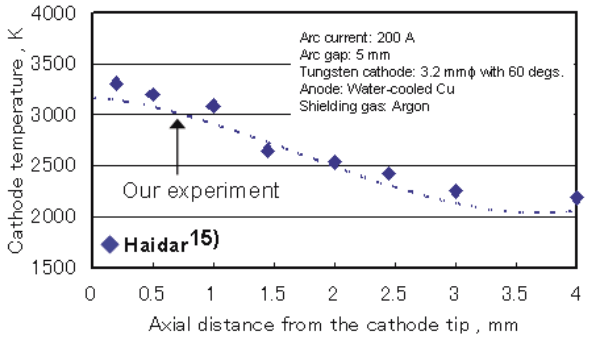

Fig. 4 Distribution of tungsten electrode surface temperature measured with high-speed temperature measurement system by two-color pyrometry.

3. Visualization of temperature distribution of molten metal in Gas Metal Arc welding

3.1 Droplet temperature in CO_2 arc welding

It is difficult to conduct temperature measurement with high accuracy, because the droplet as the anode is covered with the arc plasma. Therefore, the arc current was decreased to 0~40A momentarily at a frequency of 5Hz and the droplet temperature was measured just after the arc vanished. The frame rate was 500fps.

As an example of the experimental result of droplet temperature measurement in CO_2 arc welding, the droplet image (950nm) and 2D distribution of droplet surface temperature just after the arc vanished in the case of an arc current of 330A and wire feed rate of 12.5 m/min are shown in **Figure 5**. It is clear that heat input into the droplet increases due to constriction of the arc is caused by the thermal pinch effect in CO_2 arc welding and, consequently, the droplet temperature increases locally in the bottom region (the arc root region). The maximum temperature seen in the bottom region reaches 2900~3300K which is nearly the same level as the boiling point of iron. On the other hand, the upper region is as the relatively lower temperature of 2000~2400K. As a result, it was found that the temperature gradient reaches approximately 500K/mm in the droplet. **Figure 6** shows time variation of droplet temperature distribution from 2ms to 10ms after the arc vanished. High temperature region seen in the bottom part of the droplet just after the arc vanished moves to the left part and is reduced at 2ms. Furthermore, the high temperature region gradually moves to the upper part due to inertia and convection in the droplet. At 10ms, the droplet temperature is 2200～2600K and the temperature distribution becomes uniform.

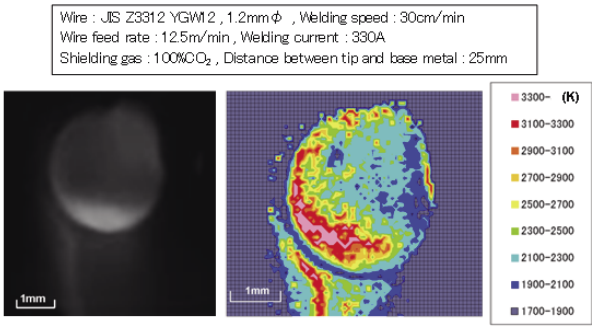

Fig. 5 Droplet temperature in CO_2 arc welding.

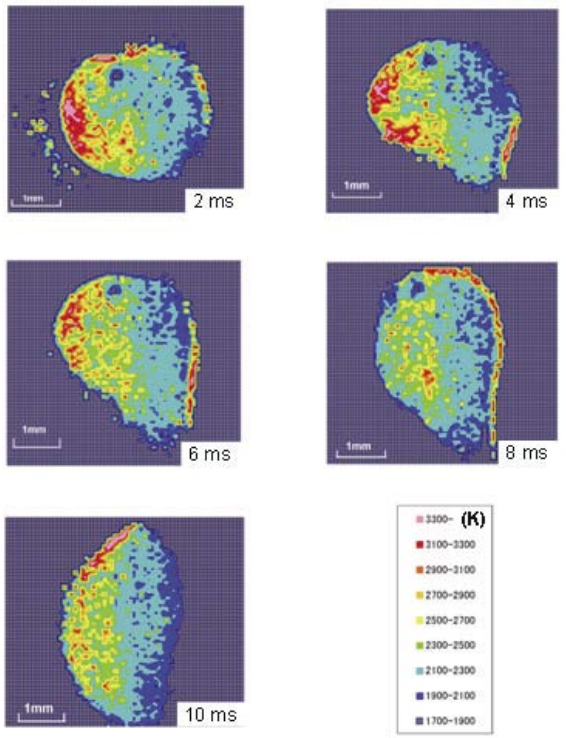

Fig. 6 Time variation in droplet temperature in CO_2 arc welding.

3.2 Droplet temperature in MAG (Ar-20%CO_2) welding

As an example of the experimental result of droplet temperature measurement in MAG welding, 2D distribution of droplet surface temperature just after the arc was vanished in the case of arc current of 280A and wire feed rate of 9.5 m/min are shown in **Figure 7**. The droplet is smaller than that of CO_2 arc welding and the transfer mode becomes spray transfer. Locally high temperature region as shown in the case of CO_2 arc

welding was not seen because the arc covers the entire droplet. Consequently, the average droplet temperature is approximately 2300K and the temperature distribution becomes uniform.

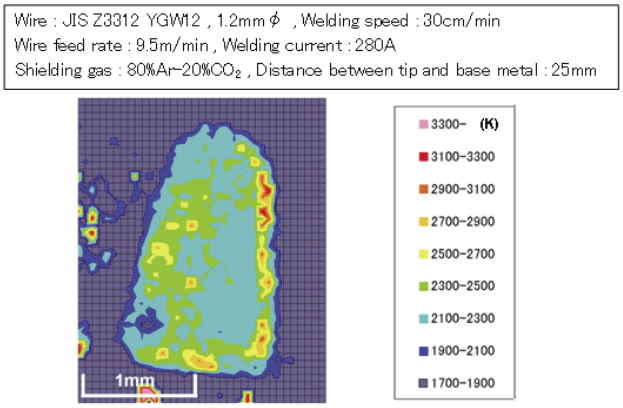

Fig. 7 Droplet temperature in MAG welding.

3.3 Weld pool temperature in CO_2 arc welding and MAG (Ar-20%CO_2) welding

It is difficult to conduct temperature measurement with high accuracy, because the weld pool as a cathode is covered with the arc plasma. Therefore, the arc current was decreased to 0~40A momentarily at a frequency of 5Hz and the weld pool temperature was measured just after the arc vanished. The frame rate was 125fps.

As an example of the experimental result of weld pool temperature measurement in MAG welding, the weld pool image (950nm) and 2D distribution of droplet surface temperature just after the arc vanished in the case of an arc current of 280A and wire feed rate of 30 cm/min are shown in **Figure 8**. It is seen that the temperature distribution becomes uniform and the temperature is 1715 K～1845 K, which is obviously lower than that of the droplet. For this reason, it is considered that the convection velocity on the weld pool surface and in the weld pool is large and, consequently, heat input from the arc is transported to the back of the weld pool due to this convection. It is supposed that the edge of the weld pool below the arc becomes high temperature compared with the central part of the weld pool due to the influence of high speed convection.

Finally, the weld pool temperature in CO_2 arc welding is shown in **Figure 9**. It is seen that the temperature distribution becomes uniform and the temperature is 1780 K～1845 K which is slightly higher than that of MAG welding. It seems that surface temperature of the weld pool increases compared with that of MAG welding, since the arc is constricted due to the thermal pinch effect in CO_2 arc welding. Furthermore, a high temperature region appears near the edge of the weld pool, not below the arc but downstream of the arc. It is supposed that the heat input from the arc is transported to the downstream part of the weld pool.

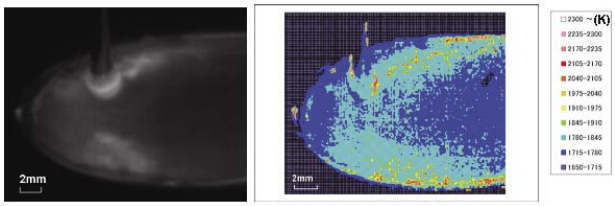

Fig. 8 Weld pool temperature in MAG welding.

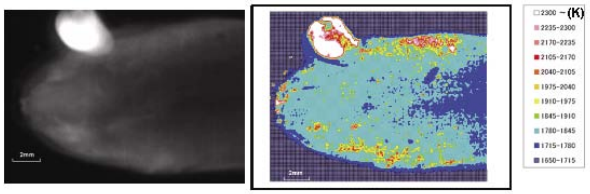

Fig. 9 Weld pool temperature in CO_2 arc welding.

4. Conclusions

Visualizations of 2D temperature distribution of molten metal in arc welding process were conducted. In CO2 arc welding, the 2D temperature distribution of the metal droplet is not uniform, namely, ranging from 2000 K to over 3000 K, while the 2D temperature distribution of the weld pool is more uniform, about 1800 K. It was found that there is a great difference between the temperature of the metal droplet and that of the weld pool in the GMA welding process.

References

1) Okagaito T, Ohji T and Miyasaka F; Quarterly Journal of the Japan Welding Society, 2005; 23: p.536-540.
2) Mishin J et. al.; J. Phys. E: Sci. Instrum. 1987; 20: p.620-625.
3) Vardelle M et. al.; Meas. Sci. Technol., 1994; 5: p.205-212.
4) Hirata Y, Ozawa T, Hamaguchi A, Kitamoto K and Ohji T; Journal of High Temperature Society, 1999; 25: p.232-238.
5) Vattulainen J et. al.; J. Thermal Spray Tech., 2001; 10(1): p.94-104.
6) Fincke JR et. al.; J. Thermal Spray Tech., 2001; 10(2): p.255-266.
7) Moreau C et. al.; Meas. Sci. Technol., 1990; 1: p.807-814.
8) Krauss M et. al.; Mater. Sci. & Eng. A, 2002; 326: p.154-164.
9) Tanaka M; Journal of The Japan Welding Society, 2004; 73: p.113-118.
10) Tashiro S, Tanaka M, Nakata K, Iwao T, Koshiishi F, Suzuki K and Yamazaki K; Quarterly Journal of the Japan Welding Society, 2006; 24: p.143-148.
11) Yamamoto K, Tanaka M, Tashiro S, Nakata K, Yamazaki K, Yamamoto E and Suzuki K; Quarterly Journal of the Japan Welding Society, 2007; 25: p.443-449.
12) Tong H, Nakata K, Tanaka M and Ushio M; Quarterly Journal of the Japan Welding Society, 2004; 22: p.375-388.
13) Yamamoto T, Yamazaki Y, Tsuji Y, Miyasaka F and Ohji T; Quarterly Journal of the Japan Welding Society, 2005; 23: p.71-76.
14) Haidar J et. al.; Rev. Sci. Instrum., 1993; 64: p.542-547.
15) Haidar J et. al.; J. Phys. D: Appl. Phys., 1995; 28: p.2089-2094.
16) Zhou X et. al.; Plasma Chem. & Plasma Process., 1996; 16: p.229S-244S.